The Astrophysical Journal Letters, 920:L19 (6pp), 2021 October 10 https://doi.org/10.3847/2041-8213/ac2aa3

Star Formation Histories of Ultra-faint Dwarf Galaxies: Environmental Differences between Magellanic and Non-Magellanic Satellites?*

Elena Sacchi[1,2,3], Hannah Richstein[4], Nitya Kallivayalil[4], Roeland van der Marel[1,5], Mattia Libralato[6], Paul Zivick[4], Gurtina Besla[7], Thomas M. Brown[1], Yumi Choi[1], Alis Deason[8,9], Tobias Fritz[10,11], Marla Geha[12], Puragra Guhathakurta[13], Myoungwon Jeon[14], Evan Kirby[15,16], Steven R. Majewski[4], Ekta Patel[17,18], Joshua D. Simon[19], Sangmo Tony Sohn[1], Erik Tollerud[1], and Andrew Wetzel[20]

[1] Space Telescope Science Institute, 3700 San Martin Drive, Baltimore, MD 21218, USA
[2] Leibniz-Institut für Astrophysik Potsdam, An der Sternwarte 16, D-14482 Potsdam, Germany; esacchi@aip.de
[3] INAF–Osservatorio di Astrofisica e Scienza dello Spazio di Bologna, Via Gobetti 93/3, I-40129 Bologna, Italy
[4] University of Virginia, Department of Astronomy, 530 McCormick Road, Charlottesville, VA 22904, USA
[5] Center for Astrophysical Sciences, Department of Physics & Astronomy, Johns Hopkins University, Baltimore, MD 21218, USA
[6] AURA for the European Space Agency (ESA), ESA Office, Space Telescope Science Institute, 3700 San Martin Drive, Baltimore, MD 21218, USA
[7] Steward Observatory, University of Arizona, 933 North Cherry Avenue, Tucson, AZ 85721-0065, USA
[8] Institute for Computational Cosmology, Department of Physics, University of Durham, South Road, Durham DH1 3LE, UK
[9] Centre for Extragalactic Astronomy, Department of Physics, University of Durham, South Road, Durham DH1 3LE, UK
[10] Instituto de Astrofísica de Canarias, Calle Via Láctea s/n, E-38206, La Laguna, Tenerife, Spain
[11] Universidad de La Laguna (ULL), Departamento de Astrofísica, E-30206, La Laguna, Tenerife, Spain
[12] Department of Astronomy, Yale University, 52 Hillhouse Avenue, New Haven, CT 06520, USA
[13] UCO/Lick Observatory, Department of Astronomy & Astrophysics, University of California Santa Cruz, 1156 High Street, Santa Cruz, CA 95064, USA
[14] School of Space Research, Kyung Hee University, 1732 Deogyeong-daero, Yongin-si, Gyeonggi-do 17104, Republic of Korea
[15] Department of Astronomy, California Institute of Technology, 1200 E California Boulevard, Pasadena, CA 91125, USA
[16] Department of Physics, University of Notre Dame, Notre Dame, IN 46556, USA
[17] Department of Astronomy, University of California, Berkeley, 501 Campbell Hall, Berkeley, CA, 94720, USA
[18] Miller Institute for Basic Research in Science, 468 Donner Lab, Berkeley, CA 94720, USA
[19] Observatories of the Carnegie Institution for Science, 813 Santa Barbara Street, Pasadena, CA 91101, USA
[20] Department of Physics & Astronomy, University of California, Davis, CA 95616, USA
Received 2021 August 9; revised 2021 September 27; accepted 2021 September 27; published 2021 October 8

Abstract

We present the color–magnitude diagrams and star formation histories (SFHs) of seven ultra-faint dwarf galaxies: Horologium 1, Hydra 2, Phoenix 2, Reticulum 2, Sagittarius 2, Triangulum 2, and Tucana 2, derived from high-precision Hubble Space Telescope photometry. We find that the SFH of each galaxy is consistent with them having created at least 80% of the stellar mass by $z \sim 6$. For all galaxies, we find quenching times older than 11.5 Gyr ago, compatible with the scenario in which reionization suppresses the star formation of small dark matter halos. However, our analysis also reveals some differences in the SFHs of candidate Magellanic Cloud satellites, i.e., galaxies that are likely satellites of the Large Magellanic Cloud and that entered the Milky Way potential only recently. Indeed, Magellanic satellites show quenching times about 600 Myr more recent with respect to those of other Milky Way satellites, on average, even though the respective timings are still compatible within the errors. This finding is consistent with theoretical models that suggest that satellites' SFHs may depend on their host environment at early times, although we caution that within the error bars all galaxies in our sample are consistent with being quenched at a single epoch.

Unified Astronomy Thesaurus concepts: Dwarf galaxies (416); Galaxy evolution (594); Galaxy dynamics (591); Galaxy stellar content (621); Galaxy kinematics (602); Star formation (1569); Local Group (929); Magellanic Clouds (990)

1. Introduction

Ultra-faint dwarf (UFD) galaxies are interesting and peculiar objects, representing many extremes in terms of galaxy properties. Their population includes the least luminous, least chemically enriched, most dark matter (DM) dominated, and oldest satellite galaxies of the Milky Way (MW; Simon 2019). UFDs could be the relics of the first galaxies believed to form, and therefore provide us with a fossil record of the conditions for star formation in the era of reionization (Bovill & Ricotti 2009 and references therein). According to the prevailing Lambda Cold Dark Matter (ΛCDM) cosmological scenario, an important channel for mass growth of DM halos is hierarchical accretion. Indeed, simulations show that even low-mass host halos have substructures down to their resolution limit (Wetzel et al. 2016; Dooley et al. 2017; Besla et al. 2018; Jahn et al. 2019; Wang et al. 2020). UFDs would also undergo hierarchical growth, and are thus precious tools to study the physics of galaxy assembly in the early universe.

Recent simulations have illustrated in detail that star formation (SF) in UFDs is impacted by the local background UV ionizing field and stellar feedback, with both acting as effective quenching mechanisms at such low-mass scales (e.g., Jeon et al. 2017, 2021; Wheeler et al. 2019; Applebaum et al. 2021). The timescales in these simulations are such that shortly after the epoch of reionization ends ($z \sim 6$), UFDs are effectively quenched; though, the exact duration of SF can vary depending on the halo mass, even for a fixed ionization

* Based on observations obtained with the NASA/ESA Hubble Space Telescope at the Space Telescope Science Institute, which is operated by the Association of Universities for Research in Astronomy under NASA Contract NAS 5-26555.

Table 1
Properties of the Seven UFD Galaxies Analyzed Here

Galaxy	Abbreviation	l (deg)	b (deg)	d (kpc)	DM	$N_\star$	$M_\star$ ($M_\odot$)	M_V	A_V	⟨[Fe/H]⟩	MC Satellite?
Horologium 1	Hor 1	270.9	−54.7	83.2	19.60	483	1.96×10^3	−3.4	0.04	−2.76	yes
Hydra 2	Hya 2	295.6	30.5	150.7	20.89	334	7.10×10^3	−4.8	0.17	−2.02	
Phoenix 2	Phx 2	323.3	−60.2	80.0	19.52	284	1.13×10^3	−2.8	0.03	−2.51	yes
Reticulum 2	Ret 2	265.9	−49.6	31.6	17.50	237	1.00×10^3	−2.7	0.05	−2.46	yes
Sagittarius 2	Sag 2	18.9	−22.9	66.1	19.10	2199	2.47×10^3	−5.2	0.34	−2.81	
Triangulum 2	Tri 2	140.9	−23.8	28.4	17.27	237	8.97×10^2	−1.8	0.22	−2.38	
Tucana 2	Tuc 2	327.9	−52.8	57.5	18.80	158	4.90×10^3	−3.8	0.05	−2.23	

Note. Columns 1 and 2 list the galaxy names, columns 3 and 4 list the galactocentric coordinates, columns 5 and 6 list the distance from the Sun (in kiloparsecs) and distance modulus (Fritz et al. 2018, 2019, and references therein), column 7 lists the number of stars used in this study, column 8 lists the estimated stellar mass (Sales et al. 2017 and references therein; for cases without estimates of $M_\star$, it was derived from the listed V-band magnitude assuming a mass-to-light ratio $\Upsilon = 2$ in solar units), column 9 lists the V-band magnitude, column 10 lists the V-band extinction, and column 11 lists the average metallicity (Fritz et al. 2018, 2019, and references therein). The last column indicates whether a galaxy is a potential Magellanic satellite, according to the analyses in Erkal & Belokurov (2019) and Patel et al. (2020).

background (Jeon et al. 2017), and often some residual interstellar medium remains in the galaxies and can fuel SF for another 1–2 Gyr (Wheeler et al. 2019). Analyses of zoom-in simulations of UFDs in MW-like environments have found that traditional environmental effects (e.g., tidal field and ram pressure) are not primary factors in the quenching timescale (Applebaum et al. 2021).

Observational data support a ubiquitous quenching timescale for UFDs around the time of reionization (Brown et al. 2014; Weisz et al. 2014). Given that the MW accreted these systems at different times (Fritz et al. 2018), this indicates a global rather than a local physical explanation for the common quenching timescale. However, other studies (e.g., Joshi et al. 2021) have shown a dependence of the quenching timescale on host mass, presumably because the strength of the background and local UV field changes depending on the environment (more massive hosts would have more SF and thus produce more ionizing radiation). However, this study explores the mass range of $10^{7-10}\ M_\odot$, thus their results might not hold for the lower-mass galaxies we are interested in.

UFDs are hard to identify due to their low luminosities $M_V > -8$, implying stellar masses $M_\star \lesssim 10^4\ M_\odot$, and generally old (>10 Gyr) stellar populations (Simon 2019), which lack bright young stars that would ease their discovery and identification. However, a great effort has been made in the past few years to increase the statistics of satellites around the MW, and many new UFDs were discovered thanks to wide-field surveys such as PAN-STARRS (Laevens et al. 2015), DES (Bechtol et al. 2015; Drlica-Wagner et al. 2015; Koposov et al. 2015), and ATLAS (Torrealba et al. 2016).

Many of these new satellites were found in the proximity of the Magellanic Clouds (MC), a region targeted by several deep imaging surveys (e.g., Drlica-Wagner et al. 2015; Martin et al. 2015; Nidever et al. 2017; Koposov et al. 2018; Torrealba et al. 2018). These surveys provide a great opportunity to test the self-similarity of ΛCDM, which predicts that MW satellites, such as the Large Magellanic Cloud (LMC), should also have their own satellites, which fell into the MW potential with the whole Magellanic system (e.g., D'Onghia & Lake 2008; Sales et al. 2011; Deason et al. 2015; Jahn et al. 2019). One way to test association is to reconstruct their 3D kinematics and orbital history, which is now possible thanks to detailed proper motion (PM) measurements enabled by the Gaia mission.

Kallivayalil et al. (2018) analyzed the PMs and radial velocities of 13 UFDs using Gaia data release (DR) 2, compared their kinematics to the tidal debris of a simulated analog of the LMC, and found four UFDs whose kinematics are compatible with the LMC debris, Carina 2, Carina 3, Horologium 1, and Hydrus 1. Using a different technique, Erkal & Belokurov (2019) used Gaia DR2 PMs to rewind the satellite orbits from their present day positions and determine which ones were originally bound to the LMC; of the 25 analyzed UFDs they concluded that six, Carina 2, Carina 3, Horologium 1, Hydrus 1, Reticulum 2, and Phoenix 2, are highly compatible with a Magellanic origin. Recently, Patel et al. (2020) calculated the orbital histories of 13 ultra-faint satellites including the combined potential of the MW, LMC, and Small Magellanic Cloud (SMC) for the first time; in this scenario, they identified Carina 2, Carina 3, Horologium 1, and Hydrus 1 as long-term Magellanic satellites, and Reticulum 2 and Phoenix 2 as recently captured Magellanic satellites.

Although these works provide fundamental contributions to our understanding of the MW satellites' dynamics, we need star formation histories (SFHs) to fully explore their properties and understand the impact of environment and reionization on such low-mass galaxies. Within the Local Group, the Hubble Space Telescope (HST) is able to resolve individual stars in galaxies down to several magnitudes below the oldest main-sequence (MS) turnoff, allowing us to measure their ancient SFHs and explore differences in the SF quenching behavior (as in, e.g., Brown et al. 2014). A detailed analysis and comparison of UFDs residing in different environments at early times is also one way to discover variations in the ionization field over large scales.

Here we present an analysis of the optical color–magnitude diagrams (CMDs) and SFHs of seven UFD galaxies part of the HST Treasury Program 14734 (PI: Kallivayalil). They are listed in Table 1, together with their distances, in the range ∼30–150 kpc, V-band magnitudes, between −1.8 and −5.2, and possible association with the Magellanic Clouds. Our analysis is based on high-precision photometry from the Advanced Camera for Surveys (ACS) and literature spectroscopic measurements, and employs the synthetic CMD method to derive the SFH of each galaxy.

2. Data and Photometry

Observations of a total of 30 UFDs were performed using the F606W and F814W filters of the HST ACS Wide Field Channel (Treasury Program 14734; PI: Kallivayalil). The basic observing strategy included collecting four dithered 1100 s exposures in both filters for each target.

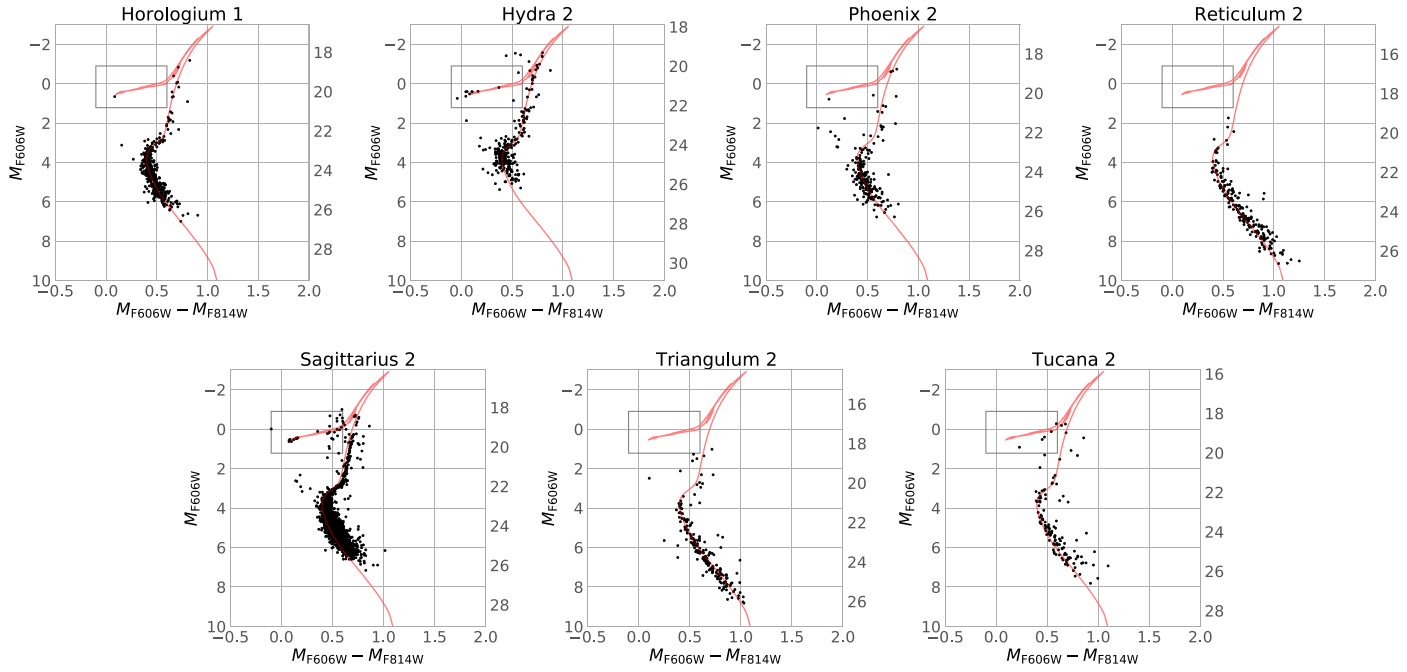

Figure 1. Color–magnitude diagrams (M_{F606W} vs. $M_{F606W} - M_{F814W}$ in Vegamag) of the seven galaxies we analyzed. The gray box shows the approximate location of the HB feature. The red line is a reference isochrone with age = 13.7 Gyr and [Fe/H] = −2.0 from the MESA/MIST library (Dotter 2016). The right *y*-axis shows the range of apparent magnitudes spanned by each galaxy. The foreground/background contamination will be accounted for in the CMD modeling phase.

The images were processed through the current ACS pipeline, which corrects for charge transfer inefficiency (CTI), and the separate dithers were combined using the DRIZZLE package to create the drc files. The CTI-corrected separate dither images, or flc files, were also used to create the photometric catalogs. The photutils routines `DAOStarFinder` and `aperture_photometry` were used to detect sources and to calculate the flux inside circular apertures of both four- and six-pixel radii. We imposed two separate criteria to create a flag differentiating real sources from artifacts. First, we tracked whether a given source's magnitude in the four- and six-pixel radii was within 1.5 standard deviations of the median difference across all sources. The second criterion was that the magnitude difference between the two radii must be positive. Sources meeting both conditions were flagged as real. We performed encircled energy corrections and converted the flux to STMAG. The four-pixel radius drc magnitudes for each matching source between filters were used in the final photometric catalogs. Lastly, magnitudes were converted to the Vegamag photometric system.

Sources in the flc images underwent the same steps and were matched across the four separate dithers in each filter using a six-parameter linear transformation. To derive an empirical error in the mean magnitude for the sources, we used the sigma-clipped standard deviation of the four-pixel radius flc magnitudes for each source in the separate filters. The flc sources were then matched between the filters before being matched to the drc sources using the same six-parameter transformation method.

We analyze here the UFDs in the program with enough stars (at least 100) to perform a reliable CMD fit; for less populated CMDs, random uncertainties due to stochastic sampling of the CMD become critical and affect the reliability of the fitting technique.

We include Sag 2 in our sample, though there is conflicting evidence of it being either a UFD (Longeard et al. 2020) or a globular cluster (Mutlu-Pakdil et al. 2018; Longeard et al. 2021); spectroscopic follow-up observations would be the ultimate confirmation of its true nature.

3. Color–magnitude Diagrams

Figure 1 presents the M_{F606W} versus $M_{F606W} - M_{F814W}$ CMDs of the UFD galaxies analyzed here. We show absolute magnitudes, derived according to the appropriate distance and extinction (as in Table 1), to ease the comparison among galaxies (apparent magnitudes are on the right *y*-axis). The gray box shows the approximate location of the horizontal branch (HB), the core He-burning evolutionary phase of stars with masses $\lesssim 2\ M_{\odot}$ and low metallicity ([Fe/H] < -1.5), while the red line is a reference isochrone with age = 13.7 Gyr and [Fe/H] = −2.0 from the MESA/MIST library (Dotter 2016).

These CMDs are dominated by an ancient metal-poor population, and we can identify the oldest MS turnoff at $M_{F606W} \sim 3$ and $M_{F606W} - M_{F814W} \sim 0.5$, which is our most sensitive and reliable age constraint. Using the isochrone as a guide, we also notice how the color, color spread, and turnoff morphology vary slightly from galaxy to galaxy, indicating their different SF and chemical evolution histories.

A few galaxies, particularly Hya 2 and Sag 2, show an extended HB, reaching very blue colors, while Hor 1 and Phx 2 may have a single blue HB candidate. The current empirical and theoretical evidence indicates that the HB morphology is affected by the initial metal content, with more metal-poor populations showing bluer HBs. However, there might be other, more complicated parameters affecting the HB morphology, and the modeling of this phase is still subject to great uncertainties (see, e.g., Torelli et al. 2019).

There are a few blue straggler stars in some of the CMDs, extending at bluer colors and brighter magnitudes than the dominant MS turnoff. This is particularly evident in Phx 2 and Sag 2. These stars are very common in ancient populations

(Santana et al. 2013), but they can mimic a much younger subpopulation. For example, the turnoff mass at 12–13 Gyr is $\sim 0.8\,M_{\odot}$, but blue stragglers can be even twice as massive, resembling an MS population of ~ 2 Gyr. This is why we exclude them from the CMD fitting (see Section 4).

4. Star Formation History Derivation

To date, the most powerful approach to recovering an SFH from an observed CMD is the comparison with models, a method applied by many different groups (see, e.g., the review by Tolstoy et al. 2009). Synthetic CMDs are built from a set of stellar models (evolutionary tracks or isochrones) adequately treated to match the distance, extinction, and photometric properties of the galaxy under analysis. To add the right scatter to the models, we adopt a scattering function based on fitting the photometric errors generated by the photometry pipeline (see Section 2). Each synthetic CMD represents a simple stellar population of fixed age and metallicity, and a linear combination of these creates a composite population that can represent, with the appropriate weights, any SFH. The best-fitting weights are determined by using a minimization algorithm to compare data and models. To take into account the effect of field contamination, we include an additional component built from the Besançon Galaxy model (Robin et al. 2003) along the line of sight to each galaxy (as in, e.g., Brown et al. 2014).

We adopt Poisson maximum likelihood statistics to perform the minimization of the residuals between data and models, to accommodate the fact that some parts of the CMD might have a low number of stars. We implemented the construction of the synthetic CMDs and the comparison between models and data in the hybrid genetic code SFERA (Cignoni et al. 2015).

To take into account possible systematic effects due to the adopted stellar evolution models, we derive SFHs using two different sets of models, the *Victoria-Regina* library (VandenBerg et al. 2014) and the MESA/MIST library (Dotter 2016). While the MESA/MIST models are available only for scaled-solar abundances, we adopt the *Victoria-Regina* models with an enhancement of +0.4 for α-elements, which is more appropriate for old metal-poor populations. While this should represent a good approximation for UFDs, some variations are observed from galaxy to galaxy, which might introduce some uncertainty in the age estimates; however, we expect them to affect the SFHs at a much smaller level than the statistical and systematic uncertainties already taken into account in our analysis. Moreover, while various systematic uncertainties certainly affect our absolute age estimates, one of the main goals of this paper is to do a relative comparison between ages, which is more robust as systematics will affect all SFHs in the same way.

We use an isochrone grid with [Fe/H] in the range $[-1, -4]$ with 0.1 dex steps (using literature spectroscopic measurements as a further constraint), and ages in the range [8, 13.7] Gyr with 100 Myr steps. We assume a Kroupa (2001) IMF and 30% of binaries drawn from the same IMF (Spencer et al. 2017; we checked that very little differences are found when different fractions or mass ratios are adopted). Distance moduli and extinctions are taken from the literature (Table 1), but the code allows for small variations in these parameters to maximize the likelihood.

We fit the CMD sequence from the MS turnoff to the top of the subgiant branch (see the box in Figure 2), to focus on the region most sensitive to age variations, while at the same time avoiding areas that are poorly constrained by the models. Also, excluding the lower MS minimizes the sensitivity of the fit to the assumed IMF. Moreover, we avoid blue stragglers, which might mimic a much younger population as discussed in Section 3. At the faintest end of the SFH derivation the observations are near 100% complete, and the typical magnitude error is 0.01–0.02 mag, depending on the galaxy.

5. Results and Discussion

An example of the output from SFERA is shown in Figure 2 for Sag 2. Panels (a) and (b) show the Hess diagrams of the observed and recovered CMDs (the latter based on MIST models), while panel (c) shows the residuals between the two; the black box corresponds to the MS turnoff area, used as a constraint for the SFH derivation. Panel (d) shows the recovered cumulative SFHs (i.e., the fraction of total stellar mass formed prior to a given epoch) from both the MIST models (in red) and the *Victoria-Regina* models (in blue); the gray band indicates the midpoint reionization redshift with its uncertainty, $z_{\rm re} = 7.7 \pm 0.7$ (Planck Collaboration et al. 2020).

Comparing observed and synthetic CMDs demonstrates how well we reproduce the data, even when fitting only the MS turnoff area. We can also reproduce the luminosity of the HB, even though the models do not reach the most extreme blue colors; this is one of the well-known complications in HB morphology modeling.

Figure 3 (left panel) shows the cumulative SFHs for the galaxies we analyzed, with the same reference to reionization as in Figure 2. As expected, the SFHs are predominantly old, consistent with the galaxies having created at least 80% of their stellar mass by $z \sim 6$ (in agreement with, e.g., Bose et al. 2018). Table 2 summarizes the time at which 50% of the total stellar mass was formed (τ_{50}) and the time at which 90% of the total stellar mass was formed (τ_{90}, quenching time, as in, e.g., Weisz et al. 2015, 2019) by each galaxy. We adopt τ_{90} as a proxy for the quenching time to minimize possible residual contamination from blue stragglers and to ease the comparison of our results with the literature. All galaxies in our sample have quenching times older than 11.5 Gyr ago.

The middle and right panels of Figure 3 show the same results divided into two subsamples: candidate Magellanic satellites and non-Magellanic satellites, according to the results by Kallivayalil et al. (2018), Erkal & Belokurov (2019) Fritz et al. (2019), and Patel et al. (2020). For each panel, the black solid curves also show the error-weighted average SFH of the two subsamples, while the dashed gray line is the average of the other subsample. On average, we find $\tau_{90} = 12.06 \pm 0.72$ Gyr ago for Magellanic satellites and $\tau_{90} = 12.68 \pm 0.23$ Gyr ago for non-Magellanic satellites (this becomes 12.67 ± 0.41 if we exclude Sag 2); even though they are comparable within the errors, there is a marginal difference between these values (a two-sample KS test of the average distributions gives a p-value of 5.7×10^{-10}). Indeed, the candidate Magellanic satellites appear to have more prolonged SFHs compared to non-Magellanic ones, possibly due to the fact that they should have resided in low-density environments for most of their lifetimes; however, the uncertainties are too large to reach a definitive conclusion.

Another interesting consideration is that, among the non-Magellanic satellites, the one with the youngest SFH is Hya 2, i.e., the most distant one in the sample ($\sim$150 kpc, whereas all others lie within $\sim$80 kpc), and the most massive one, which is

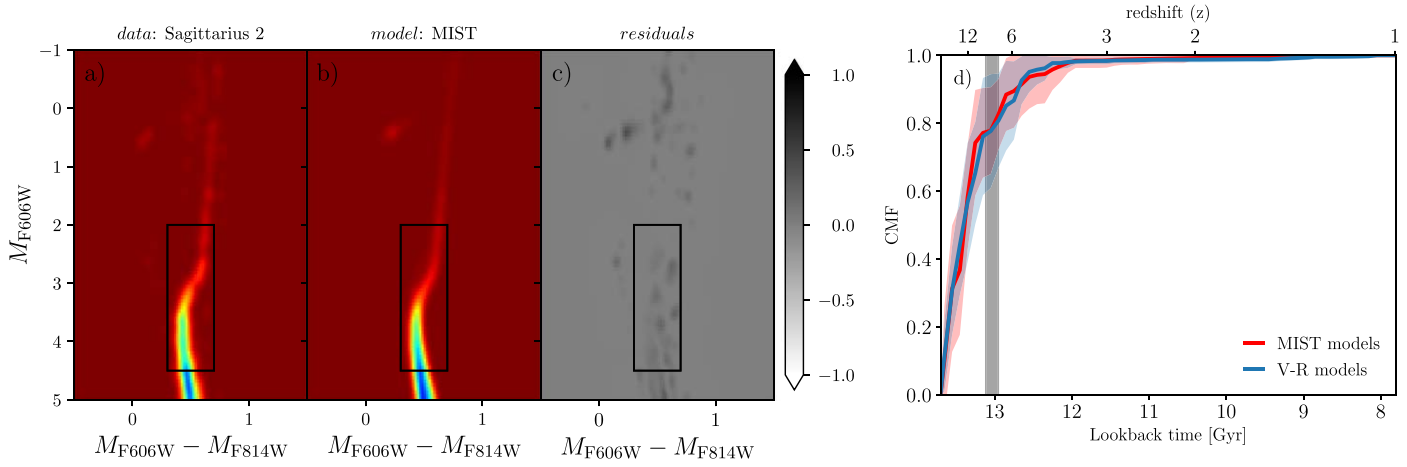

Figure 2. Example of the output from SFERA for the galaxy Sag 2. Panel (a): Hess diagram of the M_{F606W} vs. $M_{F606W} - M_{F814W}$ CMD from our data. Panel (b): Hess diagram reconstructed from the best-fit SFH on the basis of the MIST models. Panel (c): residuals between the two; the black box corresponds to the MS turnoff area, used for the fit. Panel (d): recovered cumulative SFHs (from the MIST models in red, from the *Victoria-Regina* models in blue) with 1σ uncertainties; the gray band indicates the midpoint reionization redshift $z_{re} = 7.7 \pm 0.7$ (Planck Collaboration et al. 2020).

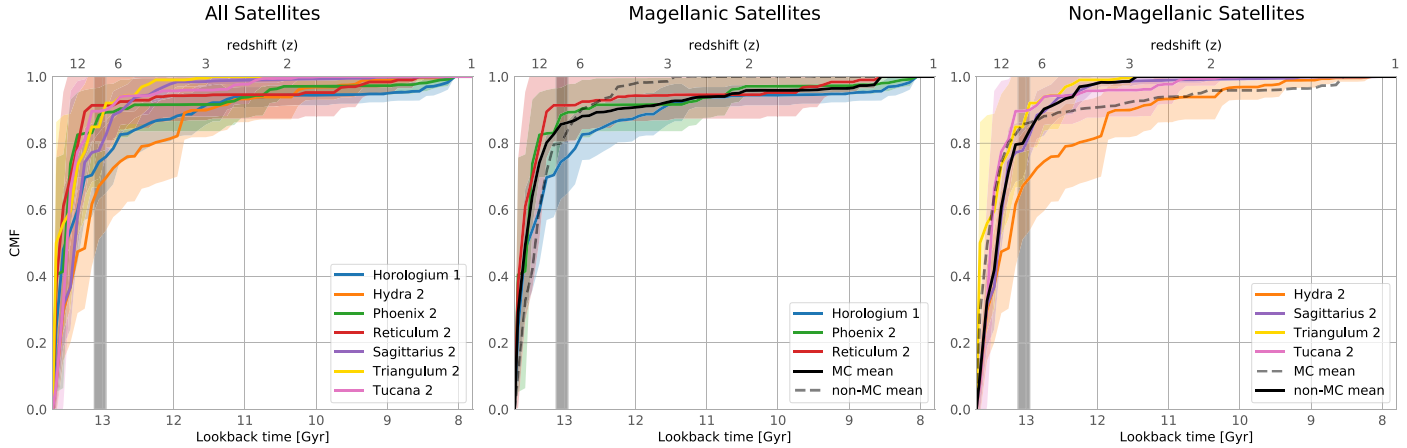

Figure 3. Left panel: cumulative SFHs of the seven UFD galaxies we analyzed, with 1σ uncertainties. The gray band indicates the midpoint reionization redshift $z_{re} = 7.7 \pm 0.7$ (Planck Collaboration et al. 2020). Middle panel: same for the candidate Magellanic satellites; the black solid line shows the error-weighted average of the subsample, while the dashed gray line shows the error-weighted average of the other subsample (non-Magellanic satellites). Right panel: same for the non-Magellanic satellites.

Table 2
Summary of the Time at which 50% of the Total Stellar Mass Was Formed (τ_{50}) and the Time at which 90% of the Total Stellar Mass Was Formed (τ_{90}, Quenching Time) for Each Galaxy

Galaxy	τ_{50} (Gyr ago)	τ_{90} (Gyr ago)	MC Satellite?
Tri 2	13.50 ± 0.23	12.91 ± 0.53	
Tuc 2	13.42 ± 0.17	12.84 ± 0.84	
Sag 2	13.40 ± 0.07	12.68 ± 0.28	
Phx 2	13.50 ± 0.14	12.47 ± 1.10	yes
Ret 2	13.52 ± 0.16	12.29 ± 1.77	yes
Hya 2	13.21 ± 0.32	11.59 ± 1.00	
Hor 1	13.44 ± 0.17	11.53 ± 1.13	yes

Note. The list is sorted by quenching time (from oldest to youngest). The last column indicates whether a galaxy is a potential Magellanic satellite (Erkal & Belokurov 2019; Patel et al. 2020).

also likely on first infall into the MWs halo (Patel et al. 2020). However, distance makes the SFH uncertainties quite large, so these results should be regarded with caution. The shape of the SFH is also different for the two subsamples, with non-Magellanic satellites reaching 100% of the stellar mass assembly within 11.5 Gyr ago, i.e., $z \sim 3$, while MC satellites show more prolonged star formation and reached the same point only 8.5 Gyr ago.

Similarly, in a study comparing the quenching times of M31 and MW satellites, Weisz et al. (2019) found that the two populations do not share many trends, though the authors do not have measurements for similar-mass UFDs in M31. Despite the uncertainties (due to the limited sample of UFDs around M31 and the fact that the satellites' distances prevent reaching the oldest MS turnoff), they suggest that a connection between the SFHs of satellites and their host galaxy's accretion history could be the best explanation for this different behavior.

These results, together with the extended SFHs we find for MC satellites, might support the idea that satellites of low-mass hosts experience a weaker ionization field, resulting in a more prolonged SFH than if they were satellites of more massive hosts, as found by, e.g., Joshi et al. (2021). On the other hand, it is important to be mindful of our uncertainties, and be cautious about overinterpreting these results. Within the error bars, all galaxies in our sample are compatible with being quenched by reionization, as found in other works (e.g., Brown et al. 2014;

Weisz et al. 2015; Tollerud & Peek 2018; Fillingham et al. 2019).

From the numerical point of view, simulations reaching the necessary resolution for UFDs have mainly examined field galaxies (e.g., Jeon et al. 2017; Wheeler et al. 2019), and find that reionization and SNe feedback are key factors to their quenching. More recently, Applebaum et al. (2021) presented a suite of cosmological simulations that contain zoom-ins of MW-like galaxies, with simulated satellites extending to the UFD regime. By comparing UFD satellites to UFDs in the field, the authors found that reionization and feedback were indeed the main quenching mechanisms, rather than environmental effects (it is worth noting that these simulations lack radiative feedback from the host galaxies and adopt a uniform reionization model). However, studies examining the SFHs of UFDs around LMC-like dwarfs are not available, yet.

Despite the challenges, studies of the kind presented here are fundamental to fully explore the properties of low-mass galaxies, and to understand the impact of environment and reionization on such systems. A detailed analysis and comparison of the SFHs of UFDs residing in different environments at early times is also a way to discover variations in the ionization field over large scales. The observations presented here will also be an important baseline for follow-up imaging with HST and the James Webb Space Telescope, to measure both bulk PMs and internal motions, while spectroscopic surveys will improve metallicity constraints (thus allowing also more precise age derivations) on these very interesting galaxies.

These data are associated with the HST Treasury Program 14734 (PI Kallivayalil). Support for this program was provided by NASA through grants from the Space Telescope Science Institute. A.W. received support from NASA ATP grant Nos. 80NSSC18K1097 and 80NSSC20K0513; a Scialog Award from the Heising-Simons Foundation; and a Hellman Fellowship. This material is based upon work supported by the National Science Foundation under grant No. AST-1847909. E.N.K. gratefully acknowledges support from a Cottrell Scholar award administered by the Research Corporation for Science Advancement.

ORCID iDs

Elena Sacchi https://orcid.org/0000-0001-5618-0109
Nitya Kallivayalil https://orcid.org/0000-0002-3204-1742
Roeland van der Marel https://orcid.org/0000-0001-7827-7825
Mattia Libralato https://orcid.org/0000-0001-9673-7397
Paul Zivick https://orcid.org/0000-0001-9409-3911
Gurtina Besla https://orcid.org/0000-0003-0715-2173
Thomas M. Brown https://orcid.org/0000-0002-1793-9968
Yumi Choi https://orcid.org/0000-0003-1680-1884
Alis Deason https://orcid.org/0000-0001-6146-2645
Tobias Fritz https://orcid.org/0000-0002-3122-300X
Marla Geha https://orcid.org/0000-0002-7007-9725
Puragra Guhathakurta https://orcid.org/0000-0001-8867-4234
Evan Kirby https://orcid.org/0000-0001-6196-5162
Steven R. Majewski https://orcid.org/0000-0003-2025-3147
Ekta Patel https://orcid.org/0000-0002-9820-1219
Sangmo Tony Sohn https://orcid.org/0000-0001-8368-0221
Erik Tollerud https://orcid.org/0000-0002-9599-310X
Andrew Wetzel https://orcid.org/0000-0003-0603-8942

References

Applebaum, E., Brooks, A. M., Christensen, C. R., et al. 2021, ApJ, 906, 96
Bechtol, K., Drlica-Wagner, A., Balbinot, E., et al. 2015, ApJ, 807, 50
Besla, G., Patton, D. R., Stierwalt, S., et al. 2018, MNRAS, 480, 3376
Bose, S., Deason, A. J., & Frenk, C. S. 2018, ApJ, 863, 123
Bovill, M. S., & Ricotti, M. 2009, ApJ, 693, 1859
Brown, T. M., Tumlinson, J., Geha, M., et al. 2014, ApJ, 796, 91
Cignoni, M., Sabbi, E., van der Marel, R. P., et al. 2015, ApJ, 811, 76
Deason, A. J., Wetzel, A. R., Garrison-Kimmel, S., & Belokurov, V. 2015, MNRAS, 453, 3568
D'Onghia, E., & Lake, G. 2008, ApJL, 686, L61
Dooley, G. A., Peter, A. H. G., Carlin, J. L., et al. 2017, MNRAS, 472, 1060
Dotter, A. 2016, ApJS, 222, 8
Drlica-Wagner, A., Bechtol, K., Rykoff, E. S., et al. 2015, ApJ, 813, 109
Erkal, D., & Belokurov, V. A. 2019, MNRAS, 495, 2554
Fillingham, S. P., Cooper, M. C., Kelley, T., et al. 2019, arXiv:1906.04180
Fritz, T. K., Battaglia, G., Pawlowski, M. S., et al. 2018, A&A, 619, A103
Fritz, T. K., Carrera, R., Battaglia, G., & Taibi, S. 2019, A&A, 623, A129
Jahn, E. D., Sales, L. V., Wetzel, A., et al. 2019, MNRAS, 489, 5348
Jeon, M., Besla, G., & Bromm, V. 2017, ApJ, 848, 85
Jeon, M., Bromm, V., Besla, G., Yoon, J., & Choi, Y. 2021, MNRAS, 502, 1
Joshi, G. D., Pillepich, A., Nelson, D., et al. 2021, MNRAS, in press
Kallivayalil, N., Sales, L. V., Zivick, P., et al. 2018, ApJ, 867, 19
Koposov, S. E., Belokurov, V., Torrealba, G., & Evans, N. W. 2015, ApJ, 805, 130
Koposov, S. E., Walker, M. G., Belokurov, V., et al. 2018, MNRAS, 479, 5343
Kroupa, P. 2001, MNRAS, 322, 231
Laevens, B. P. M., Martin, N. F., Bernard, E. J., et al. 2015, ApJ, 813, 44
Longeard, N., Martin, N., Starkenburg, E., et al. 2020, MNRAS, 491, 356
Longeard, N., Martin, N., Ibata, R. A., et al. 2021, MNRAS, 503, 2754
Martin, N. F., Nidever, D. L., Besla, G., et al. 2015, ApJL, 804, L5
Mutlu-Pakdil, B., Sand, D. J., Carlin, J. L., et al. 2018, ApJ, 863, 25
Nidever, D. L., Olsen, K., Walker, A. R., et al. 2017, AJ, 154, 199
Patel, E., Kallivayalil, N., Garavito-Camargo, N., et al. 2020, ApJ, 893, 121
Planck Collaboration, Aghanim, N., Akrami, Y., et al. 2020, A&A, 641, A6
Robin, A. C., Reylé, C., Derrière, S., & Picaud, S. 2003, A&A, 409, 523
Sales, L. V., Navarro, J. F., Cooper, A. P., et al. 2011, MNRAS, 418, 648
Sales, L. V., Navarro, J. F., Kallivayalil, N., & Frenk, C. S. 2017, MNRAS, 465, 1879
Santana, F. A., Muñoz, R. R., Geha, M., et al. 2013, ApJ, 774, 106
Simon, J. D. 2019, ARA&A, 57, 375
Spencer, M. E., Mateo, M., Walker, M. G., et al. 2017, AJ, 153, 254
Tollerud, E. J., & Peek, J. E. G. 2018, ApJ, 857, 45
Tolstoy, E., Hill, V., & Tosi, M. 2009, ARA&A, 47, 371
Torelli, M., Iannicola, G., Stetson, P. B., et al. 2019, A&A, 629, A53
Torrealba, G., Koposov, S. E., Belokurov, V., & Irwin, M. 2016, MNRAS, 459, 2370
Torrealba, G., Belokurov, V., Koposov, S. E., et al. 2018, MNRAS, 475, 5085
VandenBerg, D. A., Bergbusch, P. A., Ferguson, J. W., & Edvardsson, B. 2014, ApJ, 794, 72
Wang, J., Bose, S., Frenk, C. S., et al. 2020, Natur, 585, 39
Weisz, D. R., Dolphin, A. E., Skillman, E. D., et al. 2014, ApJ, 789, 148
Weisz, D. R., Dolphin, A. E., Skillman, E. D., et al. 2015, ApJ, 804, 136
Weisz, D. R., Martin, N. F., Dolphin, A. E., et al. 2019, ApJL, 885, L8
Wetzel, A. R., Hopkins, P. F., Kim, J.-H., et al. 2016, ApJL, 827, L23
Wheeler, C., Hopkins, P. F., Pace, A. B., et al. 2019, MNRAS, 490, 4447